EMC3-EIRENE modeling of edge plasma to improve the ICRF coupling with local gas puffing in DEMO

Wei Zhang[1,2,3,4,a)], Thomas Franke[2], Jean-Marie Noterdaeme[2,4], Dirk Van Eester[5]

[1]*Institute of Plasma Physics, Chinese Academy of Sciences, Hefei, P. R. China*
[2]*Max-Planck-Institut für Plasmaphysik, Garching, Germany*
[3]*University of Chinese Academy of Sciences, Beijing, P. R. China*
[4]*Applied Physics Department, University of Ghent, Ghent, Belgium*
[5]*Laboratory for Plasma Physics, ERM/KMS, Brussels, Belgium*

a) Corresponding author: wei.zhang@ipp.mpg.de

Abstract

We report the first 3D EMC3-EIRENE simulations of scrape-off layer (SOL) plasma in DEMO. EMC3-EIRENE is a 3D edge plasma fluid and neutral particle transport code. Effects of local gas puffing on the SOL density and Ion Cyclotron Range of Frequencies (ICRF) power coupling have been studied. A pure deuterium is simulated and the puffing/fueling gas is deuterium gas. The investigated gas puffing cases include the divertor, top, midplane and antenna gas puffing. The ICRF antenna is toroidally 360^{o} distributed and poloidally located in the outer top of the vessel. The results show that toroidal distributed but poloidal localized antenna gas puffing increases the density in front of the antenna most significantly while top or midplane gas puffing increases this antenna density to a moderate level. Influences of gas puff rate and particle transport parameters on the SOL density are investigated. The parameter scans indicate that the shift of the fast wave cut-off density position to the antenna depends almost linearly on the total gas puff rate. To achieve a significant antenna density increase, the antenna gas puff rate should be at the level of 1.8×10^{23} el/s (i.e. 1.0×10^{22} el/s per tokamak segment). As the total gas puff rate increases to 4.0×10^{23} el/s, the evanescent layer of the fast wave (with $k_{||} = 2$ m^{-1}) almost vanishes. Moreover, it is found that antenna gas puffing reduces the local power flux to the main chamber wall near the gas valve due to a local decrease of the SOL temperature.

1. Introduction

The DEMOnstration fusion power plant (DEMO) is a magnetically controlled fusion device currently under pre-conceptual design. It aims at generating hundreds of megawatt net electricity for long plasma pulses (in the level of hours) while operating with a closed fuel-cycle [1]. DEMO is considered as the final step towards commercial fusion reactor following ITER. The DEMO design used in the paper is the 2015 baseline EU-DEMO design with the following main tokamak parameters: R = 9.07 m, r = 2.93 m, κ = 1.59, δ = 0.33, plasma volume = 2502 m^3, I_p = 19.6 MA, B_0 = 5.667 T, q_{95} = 3.247, $\bar{n}_e = 7.98\times10^{19}$ m^{-3}, Z_{eff} = 2.584, H-factor = 1.1, heating power = 300 MW, P_{sep} = 150 MW, net electric power = 500MW, burn time = 2 hours.

To heat plasma to burning plasma temperature and to maintain this temperature in DEMO, robust auxiliary heating is necessary. Recent progress of heating and current drive for EU-DEMO and K-DEMO is summarized in [2] and [3], respectively. Among the heating methods, plasma heating with radio-frequency waves in the Ion Cyclotron Range of Frequencies (ICRF) is one of the standard heating methods widely used in present tokamaks, stellarators and linear devices. The main advantages of ICRF heating are its ability to achieve central power deposition at large plasma densities and directly heat the plasma ions [4, 5]. It is also very effective for non-inductive current drive in high temperature fusion reactors like DEMO. The most suitable ICRF frequency for current drive is 50MHz or 80MHz [6]. Moreover, ICRF heating can be used for ion cyclotron wall conditioning and plasma start-up [7], core impurity control [8] and sawtooth control/pacing [9, 10]. Thus, ICRF is a promising and versatile heating method in DEMO.

In recent years, it was proposed to use a traveling wave array (TWA) distributed antenna system (toroidal extension = 360°) in DEMO [11-14]. Compared to conventional antenna designs, the distributed antenna has many advantages: (1) low power density, with consequently low plasma-antenna interactions; (2) larger $k_{||}$ selectivity (narrower spectrum), thus enabling to choose the most appropriate value for plasma bulk heating and for coupling; (3) higher coupling (typically a factor 2) for a given $k_{||}$ and given strap voltage due to the absence of vertical septa between the straps; (4) no large Voltage Standing Wave Ratio (VSWR) in the feeding lines, thus eliminating the need for large size feeding lines; (5) load resilience; (6) easy and robust tuning procedure; (7) the distributed ICRF antenna can be integrated in the blanket, and only has a marginal effect on the Tritium breeding ratio [15].

Despite of the many advantages mentioned above, the ICRF antennas still have their challenges. One of the most important ones is the ICRF power coupling issue at the plasma edge due to large evanescent layer. The ICRF heating relies on the fast wave to transport the energy from the antenna to the plasmas. However, the fast wave radiating from the antenna decays exponentially in the evanescent layer where the plasma density is lower than the cut-off density in the plasma periphery. The ICRF coupling depends exponentially on the width of this layer, i.e. $R_c \propto e^{-\alpha|k_\parallel|L_{ac}}$, where R_c is the coupling resistance, L_{ac} is the width of the evanescent layer (i.e. a distance from the antenna strap to the cut-off density position), $k_\parallel$ is the parallel wave vector often prescribed by the antenna, and α is a tunneling factor that depends on the specific antenna geometry, the ICRF operating frequency and antenna array phasing. In nowadays tokamaks, the fast wave cut-off density n_{e_co} is typically in the order of 10^{17} or 10^{18} m^{-3}. This is also true for the Traveling Wave Antenna (TWA) in DEMO. The large distance between the TWA and the fast wave cut-off density leads to ICRF coupling issues in DEMO [12].

The ICRF coupling issue can be well solved by puffing fueling gas locally close to the ICRF antenna. Previous experiments and simulations on ASDEX Upgrade (AUG) [16, 17], JET [18, 19] and ITER-relevant scenario [20] indicate that compared to lower divertor gas puffing, midplane gas puffing close to the antenna increases the antenna coupling resistance to more than double (by ~120%) and top gas puffing increases this value by ~20% - 40%. No plasma confinement degradation is found when shifting the gas source from the divertor to the top or midplane of the main chamber [18, 19]. Following this, the local gas puffing technique has been extensively studied and has been routinely used to improve ICRF

coupling in tokamaks like AUG and JET. In particular, ITER is now designing two midplane gas valves close to the ICRF antennas in the equatorial plane so as to maximize the ICRF power [21]. As return of experience from AUG, JET and ITER, it is very important also for DEMO to investigate the local gas puffing method for maximization of ICRF power coupling.

This paper is dedicated to use the 3D edge plasma fluid and neutral particle transport code EMC3-ERIENE to study the SOL density during different gas puffing in DEMO. One of the major goals is to figure out the optimized gas puff location and to calculate the required gas puff rate. Various gas puffing methods, including the divertor, the top, the midplane and the antenna gas puffs, are studied. The improvement of ICRF coupling is implied by the decrease of width of evanescent layer or the shift of cut-off density position. Note that the following effects due to RF (Radio-Frequency) fields are not considered in the EMC3-EIRENE simulations: E×B drifts induced by inhomogenous RF rectified sheath potential [22, 23] and ponderomotive potential [24]; neutral ionization by near RF fields [25].

The paper is organized as follows. In section 2, the simulation configurations are discussed. They include the setups of computation grid, particle and energy transport parameters, boundary conditions and gas puffs and divertor gas pump. In section 3, the main simulation results are presented and discussed. They include effects of local gas puffing locations on SOL density (section 3.1), effects of gas puff rate on SOL density (section 3.2), effects of transport coefficient on SOL density (section 3.3) and influence of local gas puffing on particle and power fluxes to the wall (section 3.4). The main conclusions and outlooks are given in section 4.

2. Simulation configurations

EMC3-EIRENE is a code package which couples the EMC3 [26] and EIRENE [27] codes self-consistently in a 3D geometry. EMC3 solves a set of time-independent fluid equations for the mass, momentum, electron and ion energies and provides the necessary plasma parameters (density, temperature, ion/electron velocity) to EIRENE. EIRENE calculates the kinetic Boltzmann equations for neutrals and returns the source and sink terms to EMC3. Due to its 3D nature, EMC3-EIRENE has up to now been extensively used both in tokamaks and stellarators for studying 3D physics [28], such as resonant magnetic perturbation fields, localized neutral gas puffing and impurity seeding, nonsymmetrical heat loads and nonsymmetrical particle recycling fluxes. This paper presents the first results of EMC3-EIRENE modeling of local gas puff effects in DEMO.

In the simulations, a computation grid with a toroidal extension of 20^{o} (one segment) has been built (see figure 1) based on the DEMO 2015 baseline equilibrium. We have simulated only one toroidal tokamak segment because: (1) the distributed ICRF antenna is toroidal periodic; (2) the local gas valves are toroidal periodic; (3) all plasma facing components are toroidal symmetrical; (4) the resulting SOL density is toroidal periodic; and (5) the limitation of computation memory. Within one sector, the localized gas source is the only 3D feature of the simulation. In contrast, grids with a toroidal extension of 360^{o} had to be used in AUG and JET simulations [17, 18, 20] because in these machines only one or two local gas valves are used simultaneously and the resulting densities are rather toroidal inhomogenous in a large toroidal extent. The toroidal boundary of the simulation grid is defined as

follows: the plasma exiting one toroidal boundary is considered entering the simulated region from the other side. The grid in the poloidal cross-section is divided into three zones (see figure 1): core, Private Flux Region (PFR) and SOL. The SOL and PFR regions are extended to the wall. This allows the plasma profiles in the whole radial region being calculated and all recycling fluxes from the wall being considered. The additional grid region in cyan color (see figure 1) is only specified for EIRENE while all other grid domains (core, SOL and PFR) are both specified for EMC3 and EIRENE. The material of the first wall is defined as tungsten. The gas pump is approximated by setting a pump surface with a reflection coefficient of 0.96 at the bottom of the divertor. The settings of the divertor, the midplane, the top and the antenna gas puffs are also illustrated in figure 1. In the simulations, the divertor gas valves have the periodicity of the machine segments. That is to say, eighteen divertor gas valves are assumed in our simulations while only four divertor gas valves are set in the baseline EU-DEMO design [29]. The use of different number of divertor valves will however not influence the simulation results since divertor gas puffing leads to a rather homogenous SOL density. It is indicated in the simulations that the SOL density depends on the total gas puff rate but is independent on the number of divertor gas valves used.

In DEMO, the local gas valves have to be located behind the first wall like in current tokamaks so that the valves are not in direct contact with the hot plasmas. The generated gas cloud extends poloidally and toroidally after penetrating radially into the main chamber. This is reproduced by setting point gas sources backward a few centimeters from the first wall. Moreover, one local gas valve per segment has been set for every gas puffing method since the distributed antenna is toroidal 360^{o} extended. The gas valves have therefore the same toroidal periodicity as the segments. This is in contrast to the local gas valve settings in nowadays tokamak, where only one or two local gas valves at proper toroidal locations are needed in order to increase the antenna density at a specific toroidal position.

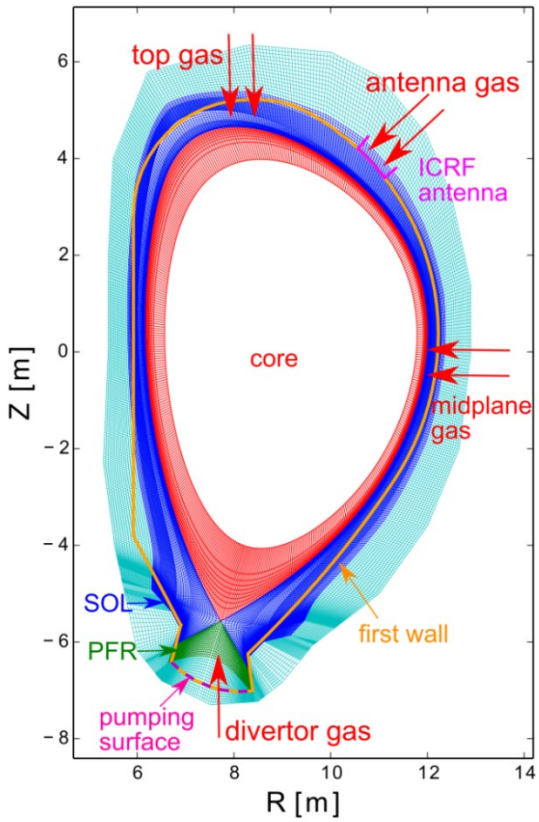

Figure 1. Poloidal cross-section of the computation grid with the first wall, gas puffs and gas pump.

In the simulations, only pure deuterium plasmas are considered for computational convenience. A change of plasma composition will change the Stix parameter R and thus the fast wave cut-off density. Here $R = 1 - \sum_s \omega_{ps}^2/[\omega(\omega + \Omega_s)]$ [30], where ω_{ps}^2 and $\Omega_s$are the plasma and cyclotron frequencies of species s, respectively. For fixed $k_{||}$, f_{ICRF} and B_0, the fast wave cut-off density in a D-T plasma is slightly smaller than that in a pure D plasma. The conclusions made for a pure D plasma would still hold for a D-T plasma. The upstream separatrix density and the total input power (i.e. the power entering the SOL) are set as $4.5 \times 10^{19}\ m^{-3}$ and 150MW, respectively. These two parameters are set as inner boundary conditions of the SOL. The outer boundary is defined by the first wall if the outermost layer of the grid exceeds the wall boundary. Otherwise, the outer boundary is defined by a decay length of ~3 cm in the outermost grid layer both for particle and energy transport, for instance the bottom part of the PFR. Transport parameters have to be prescribed in advance. For DEMO, the same particle and energy transport parameters ($D_\perp(\rho_{pol})$ and $\chi_\perp(\rho_{pol})$) as ITER [21] are used . The reasons are: firstly there is no experimental data to validate these transport coefficients; secondly, the uncertainties of the transport parameters become less important since we are calculating the relative local SOL density increase (relative to the density during divertor gas puffing); thirdly, the setting of transport parameters will have influences on the necessary gas puff rate but not on the optimized gas valve location. Nevertheless, influences of particle diffusion coefficient on SOL density are deliberately studied in section 3. Turbulence is not simulated in EMC3-EIRENE. Instead, the time average effects of particle and energy

transport caused by turbulence is considered by means of diffusion, convection and conduction in the code.

Note that due to the uncertainties in the plasma edge turbulent transport, the DEMO plasma edge profiles are themselves highly uncertain. As a consequence the associated ICRF coupling predictions cover a very wide range, which will only be sharpened once the system will start operating on the actual DEMO plasmas. The local gas puffing studies in the paper is at least an important risk mitigation measure against this type of uncertainty.

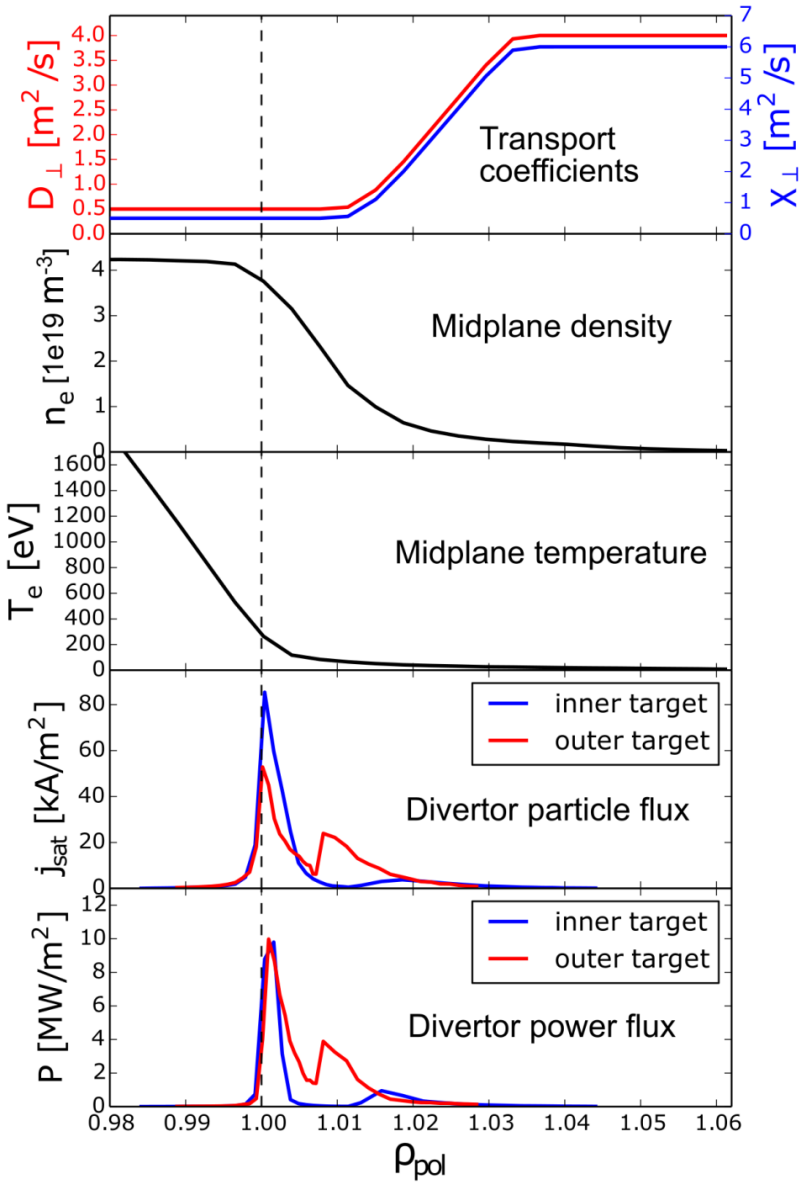

Figure 2. Plasma profiles during divertor gas puffing. From top to bottom: particle and energy transport coefficients, midplane density and temperature, particle and power fluxes to the inner and outer targets in the divertor.

The SOL upstream profiles (midplane density and temperature) and downstream profiles (particle and power fluxes to the divertor targets) during divertor gas puffing are shown in figure 2. The divertor gas puffing is used as reference throughout the paper. Similar to most tokamaks, the largest particle and power fluxes to the divertor targets are found close to the strike points. A secondary peak of power flux is seen at a radial position where the outer target is relatively close to the wall in the SOL. Note that the most important parameter for ICRF coupling is the density profile in front of the antenna, which is almost equivalent to the upstream density here as the antenna is located at the outer top of the machine.

3. Simulation results

3.1 Methodology

After running the code for the reference case and obtaining the background plasma, the gas source is then switched from the divertor to other locations of the main chamber while all other settings in the code are kept the same. The antenna density profiles in this section are averaged SOL density profiles in front of the antenna, and this average is made within the antenna range both poloidally and toroidally. The improvement of ICRF coupling is implied by the shift of the fast wave cut-off density position to the antenna since the antenna coupling resistance depends exponentially on the width of the evanescent layer.

3.2 Effects of gas puff locations on the SOL

At the fast wave cut-off in the low density region, the condition $k_0^2 R = k_{||}^2$ is satisfied. Via the Stix parameter R, the fast wave cut-off location is a function of the density and the composition of the plasma. Up to a usually negligible correction, R is proportional to the plasma density. Via $k_{||}$, it is a function of the antenna spectrum. Also the wave frequency plays a role via k_0 and R. Figure 3 - taking typical 2015 EU-DEMO parameters for the burning plasma phase - illustrates that the cut-off density for DEMO is typically a few $10^{18}\ m^{-3}$ and that it increases for increasing $k_{||}$ and/or decreasing frequency. The former is a consequence of the fact that the vacuum wave the fast wave connects to when the density becomes negligible is more deeply evanescent for higher $k_{||}$ (in vacuum, $k_0^2 = k_\perp^2 + k_{||}^2$ and hence $k_\perp \sim i k_{||}$ since k_0 is typically small w.r.t. $k_{||}$). The frequency dependence reflects that the characteristic vacuum wavelengths are shorter (k_0 is larger) when the frequency is higher. With a frequency of 50MHz, $n_{e\_co} = 0.5 \times 10^{18}\ m^{-3}$ for $k_\parallel = 2\ m^{-1}$ and $n_{e\_co} = 3.0 \times 10^{18}\ m^{-3}$ for $k_\parallel = 4\ m^{-1}$. Although coupling is good at very low values of $k_{||}$, this $k_{||}$ region is to be avoided because co-axial modes are excited there. These modes are propagative rather than evanescent but they do not penetrate the main plasma. As the power they carry remains in the edge rather than contributing to core heating, they have to be avoided.

Any adopted frequency interval when aiming at an ICRF system in DEMO that should be capable both to guarantee heating and current drive should have a frequency at which ion heating is strong and

central, while having a frequency suitable for electron heating nearby. The 50MHz window is the most suitable candidate for that. Depending on the poloidal location of the RF antenna, the higher frequency window is also a possible candidate. For top launch this is a possible suitable option since it allows to avoid excessive parasitic damping by fusion-born alpha particles by ensuring the T absorption layer stays on the high field side while the D and α absorption layer stays on the low field side of the wave's path through the plasma. In the paper, the study focuses on the ICRF frequency of 50MHz. As for the parallel wave number, the chosen values of $k_{\parallel} = 2 - 4\ m^{-1}$ are in line with values obtained in [11] on the TWA design and in [6] on the core heating and current drive physics. Note that $k_{\parallel}$ at which the TWA excites most of its power is determined both by the frequency and the strap width. Hence there is a degree of freedom to choose a particular desired value of $k_{\parallel}$ for a prescribed frequency, should this be necessary. Present thinking is that a value of $k_{\parallel,peak}$ ~ 2-3k_0 is about optimal to allow good coupling while avoiding excitation of coaxial modes which are propagating the edge rather than penetrating the plasma.

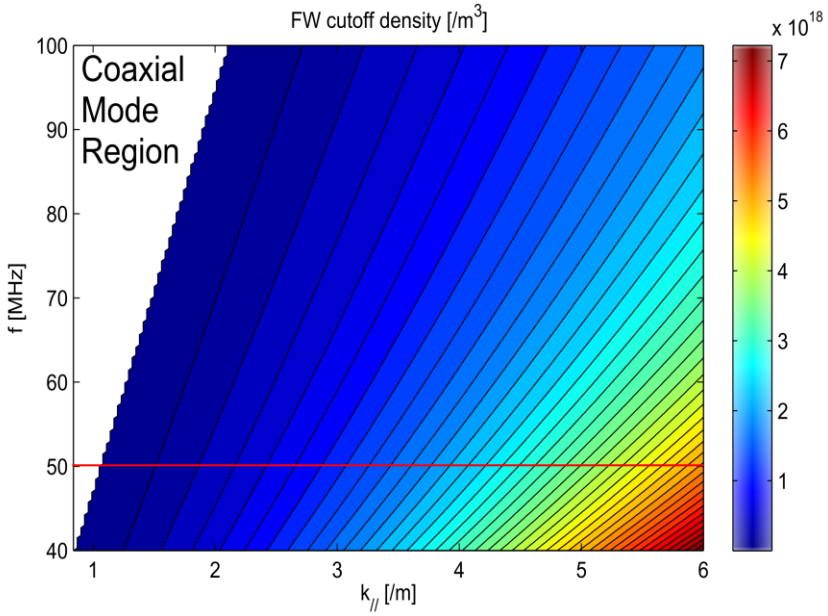

Figure 3. Fast wave cut-off density as a function of parallel wave vector $k_{\parallel}$ and ICRF heating frequency f. The red line depicts the cut-off density with f_{ICRF} = 50MHz.

One of the major aims of the work described in this paper is to figure out optimized gas valve location for maximization of ICRF coupling. For this, the divertor, midplane, top and antenna gas puffing cases have been investigated (see figure 4). The same total gas puff rate ($1.5 \times 10^{22}\ el/s$) has been used in these cases. It is shown that compared to the divertor gas puffing, the antenna gas puffing leads to the largest density increase in front of the antenna while the top or the midplane gas puffing leads to a moderate density increase. Topologically, the antenna gas valves are closest to the DEMO antenna and increase the density most significantly. In AUG and JET [17, 18], the midplane gas valves are closest to the ICRF antenna (as they are in the midplane) and leads to the largest antenna density increase. This suggests that the spatial distance from the local gas valve to the antenna plays an important role as expected.

Different local gas puffing methods lead to different localized neutral densities. Due to local ionization, the poloidal extension of increased density is strongly correlated with the poloidal spreading of the neutral gas. In fact, the largest density increase is often located poloidally close to the gas valve and the plasma cloud developed due to ionization is in the same spatial range as the neutral gas cloud. Top or midplane gas puffing leads to the largest neutral pressure increase in the top or outer midplane while the neutral pressure increase in front of the antenna is much less. In contrast, when the gas is puffed behind or close to the antenna, the gas cloud formed in the main chamber is in front of or close to the antenna. In DEMO, the designed antenna gas valves should be located behind the blanket modules. The gas has to penetrate through the gaps between the blanket modules to enter into the main chamber wall. Thus, antenna gas puffing leads to the most significant neutral density increase and thus plasma density increase in front of the antenna. In the previous studies [15, 23], it is indicated that the local density increase is attributed to the spreading of puffed neutral gas, the local ionization and the field line connections from the antenna to the local gas valves. In DEMO, the density in front of the antenna is mostly affected by the local neutral gas distribution in the same segment. This is because: (1) the ICRF antenna is toroidal 360^{o} distributed and the density increase should be toroidal 360^{o} but poloidally local in front of the antenna; (2) eighteen toroidal periodic distributed gas valves are used in all gas puff cases, so that localized neutral density cloud is develop in every segment and the poloidal locations of the gas valves play the most important role; (3) top or midplane gas puffing increase the density in the top or midplane in priority while the density increase due to remote magnetic field line connections are very limited.

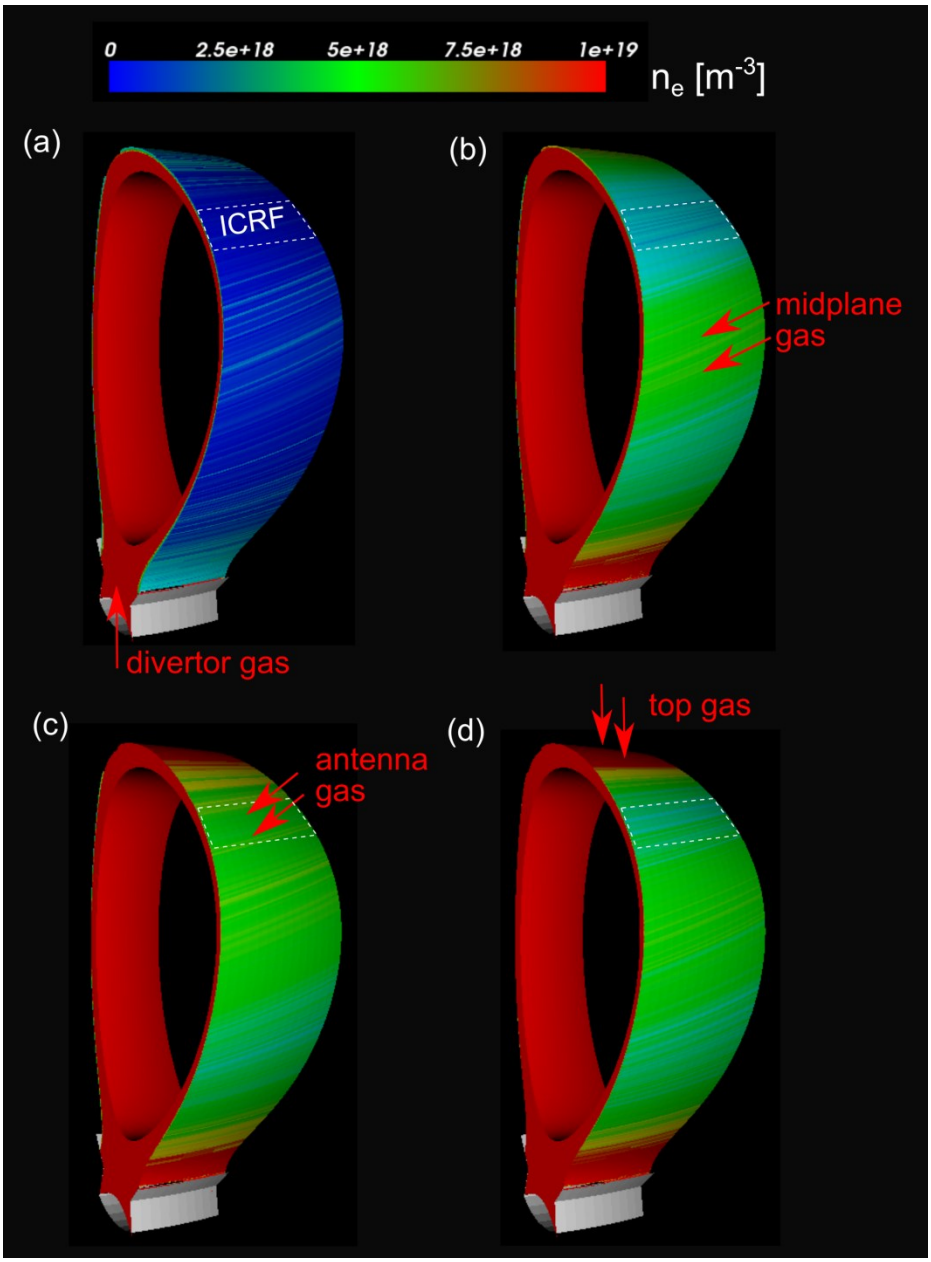

Figure 4. SOL density with the gas puff from the (a) divertor, (b) midplane, (c) antenna and (d) top. The dashed rectangle lines represent the location of the toroidal distributed ICRF antenna. The outermost SOL surface shown in the subplots is at a radial position of ρ_{pol} = 1.028. Here $\rho_{pol} = \sqrt{\psi_{pol}}$. The same total gas puff rate ($1.5 \times 10^{22}\ el/s$) is used in all cases.

To have a quantitative comparison of the antenna density, the density in front of the antenna is averaged with the formula $\langle n_e(\psi) \rangle = \frac{1}{\Delta\theta\Delta\Phi} \int_{\theta_0-\Delta\theta/2}^{\theta_0+\Delta\theta/2} \int_{\Phi_0-\Delta\Phi/2}^{\Phi_0+\Delta\Phi/2} n_e(\psi, \theta, \Phi)\, d\theta d\Phi$. Here θ_0 and Φ_0 are the poloidal and toroidal centers of the antenna; $\Delta\theta$ and $\Delta\Phi$ are the poloidal and toroidal extensions of the antenna, respectively. The results (figure 5) show quantitatively that antenna gas puffing increases the antenna density most significantly while top or midplane gas puffing increases this density only to a

moderate level. The increase of density leads to a reduction of the width of the evanescent layer and an increase of the ICRF coupling. For instance, the fast wave (with $k_{\|} = 4\ m^{-1}$) cut-off density position is shifted by ~5.0 cm towards the antenna with antenna gas puffing while it is shifted by only ~2.0 cm towards the antenna with top or midplane gas puffing. For fast wave cut-off density with $k_{\|} = 2\ m^{-1}$, this shift is ~4.9 cm with antenna gas puffing, but only ~2.1cm with top gas puffing and ~2.6cm with midplane gas puffing. In ASDEX Upgrade, a shift of 2.0 cm cut-off density position leads to an increase of ~100% ICRF power coupling in standard H-mode plasmas [17].

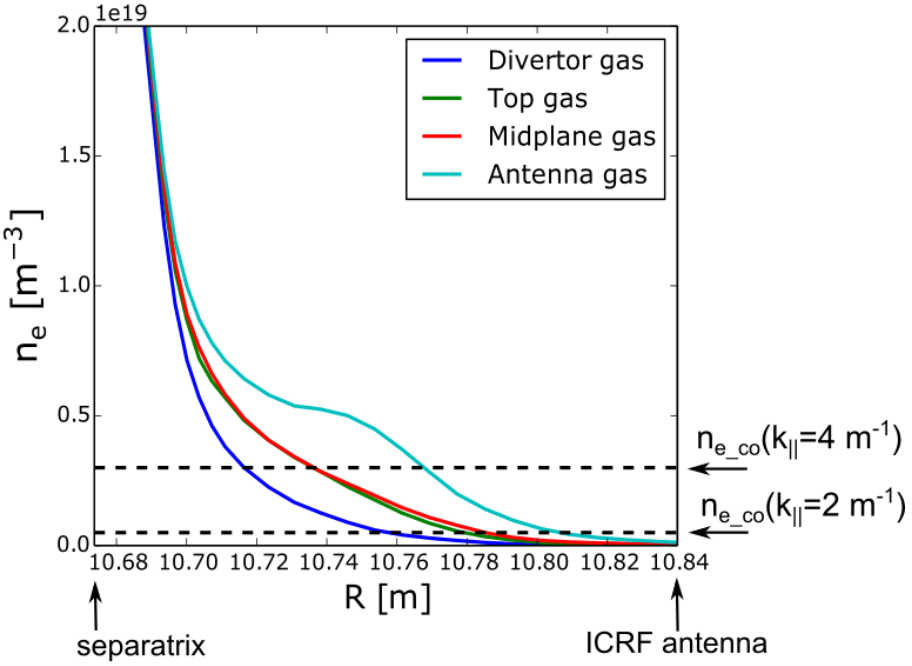

Figure 5. Averaged density profiles in front of the antenna during divertor gas puffing, top gas puffing, midplane gas puffing and antenna gas puffing. The two dashed lines represent the cut-off densities for fast waves with $k_{\|} = 4\ m^{-1}$ and $k_{\|} = 2\ m^{-1}$, respectively.

3.3 Effects of gas puff rate on density profile

Increasing the gas puff rate will further increase the density in front of the antenna. To understand the influence of gas puff rate (Φ_{D2}) on the antenna density, antenna gas puffing with a gas puff rate scan has been investigated (figure 6). The gas puff rate is increased linearly from $0.375 \times 10^{22} el/s$ to $2.25 \times 10^{22} el/s$ per segment while all other parameters in the code are kept the same. The results indicate that in order to achieve a moderate antenna density increase, the gas puff rate should be in the level of $0.375 \times 10^{22} el/s$ per segment. To obtain a significant antenna density increase, the gas puff rate has to be in the level of $1.0 \times 10^{22} el/s$ per segment (i.e. total gas puff ~$1.0 \times 10^{23} el/s$ for all segments). This total gas puff rate is of the same level as the total fueling rate in DEMO [29] but just a tiny fraction of the recycling flux as described below.

The shift of the cut-off density position (R_{shift}) depends almost linearly on the gas puff rate while the $k_{\|}L_{ac}$ value has an inverse correlation with the gas puff rate. An increase of gas puff rate decreases the width of evanescent layer L_{ac} and increases the coupled ICRF power since $P_{ICRF} \propto R_c \propto e^{-\alpha|k_{\|}|L_{ac}}$. With a gas puff rate of $\Phi_{D2} = 2.25 \times 10^{22} el/s$ per segment (total gas puff rate $\Phi_{D2} = 4.0 \times 10^{23} el/s$), the position of the fast wave cut-off density for $k_{\|} = 2\ m^{-1}$ is shifted by ~8 cm towards the antenna and the evanescent layer almost disappears. This means that the ICRF coupling issue in the plasma edge is very well solved. Thus, antenna gas puffing is a very powerful method to increase the antenna density and improving the ICRF coupling in DEMO. In AUG [17] and JET [18] H-mode, the typically used total gas puff rate (~$10^{22} el/s$) is ~6% of the total recycling flux and this amount of gas does not influence the plasma confinement. In DEMO, a total gas puff rate of $\Phi_{D2} = 4.0 \times 10^{23} el/s$ is only about 4% of the total recycling flux and we expect that this gas puff rate would not degrade the plasma confinement.

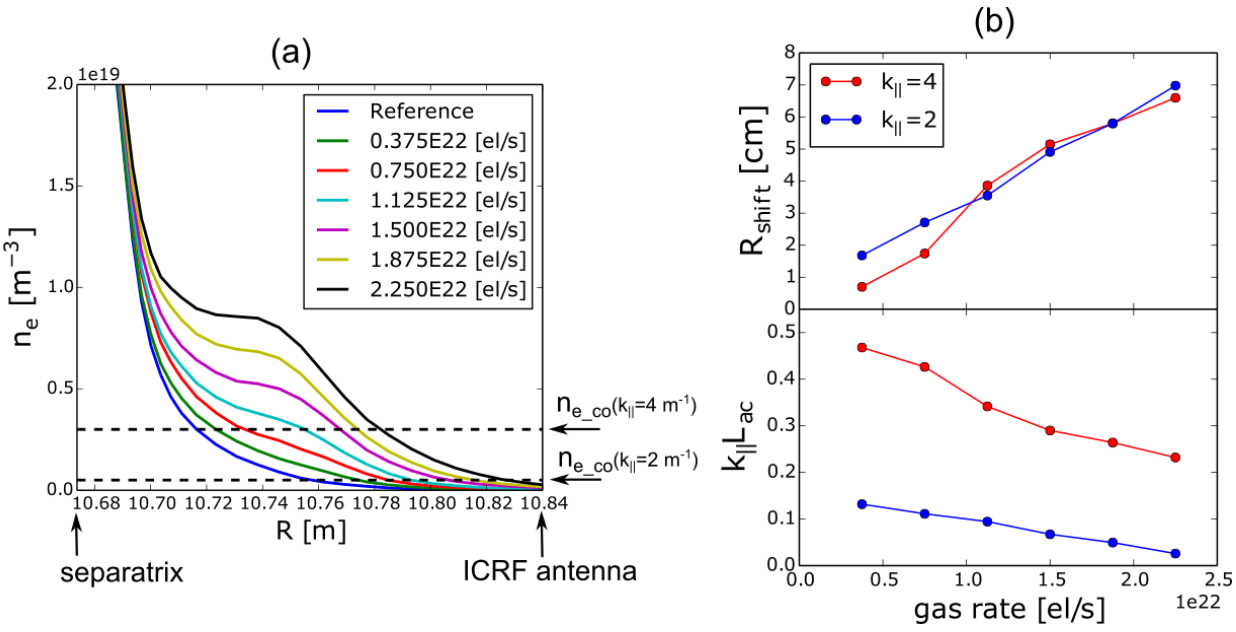

Figure 6. (a) Antenna density profiles during antenna gas puffing with different gas puff rates (gas puff rate per segment). The "reference" case represents antenna density during lower divertor gas puffing. (b) The shift of the cut-off density position (R_{shift}) and $k_{\|}L_{ac}$ as a function of gas puff rate. Here $R_{shift} = R - R_{reference}$.

It is worth mentioning that in JET we use a mix of gas injection locations to ensure (1) the RF coupling is enhanced while (2) avoiding the H-mode edge pedestal (essential for confinement) being destroyed by too massive local injection. Indeed, only a moderate gas local puffing is needed to lift the density high enough to allow the fast wave to become propagative fairly close to the antenna. It has also been experimentally demonstrated that injection too close to the antenna may not be optimal since the gas requires some time and distance to be ionized. All these points argue for a spread gas injection allowing the density close to the antenna to be lifted just above the fast wave cut-off density. To avoid risk of RF breakdown associated with gas injection, one should aim at as modest as possible gas injection. Antenna designs keeping the E-field amplitude modest - such as the TWA in DEMO - will also be of help.

3.4 Effects of transport coefficient on density profile

To understand the influence of particle transport parameter $\mathrm{D}_\perp$ on the SOL density, a scan of $\mathrm{D}_\perp$ is made for antenna gas puffing (figure 7). In this parameter scan, $\mathrm{D}_\perp$ is varied from $0.5m^2/s$ to $6.0m^2/s$ in the radial range of ρ_{pol} = [1.04, 1.06] while the total gas puff rate is the same. It is shown that when $\mathrm{D}_\perp < 4\ m^2/s$, R_{shift} appears to approach a saturated value almost exponentially as $\mathrm{D}_\perp$ increases. When $\mathrm{D}_\perp \geq 4\ m^2/s$, the density profile and R_{shift} remains almost the same as $\mathrm{D}_\perp$ increases. Overall, if $\mathrm{D}_\perp$ is overestimated, R_{shift} should be smaller than the calculated one; if $\mathrm{D}_\perp$ is underestimated, R_{shift} is should be larger than the calculated one.

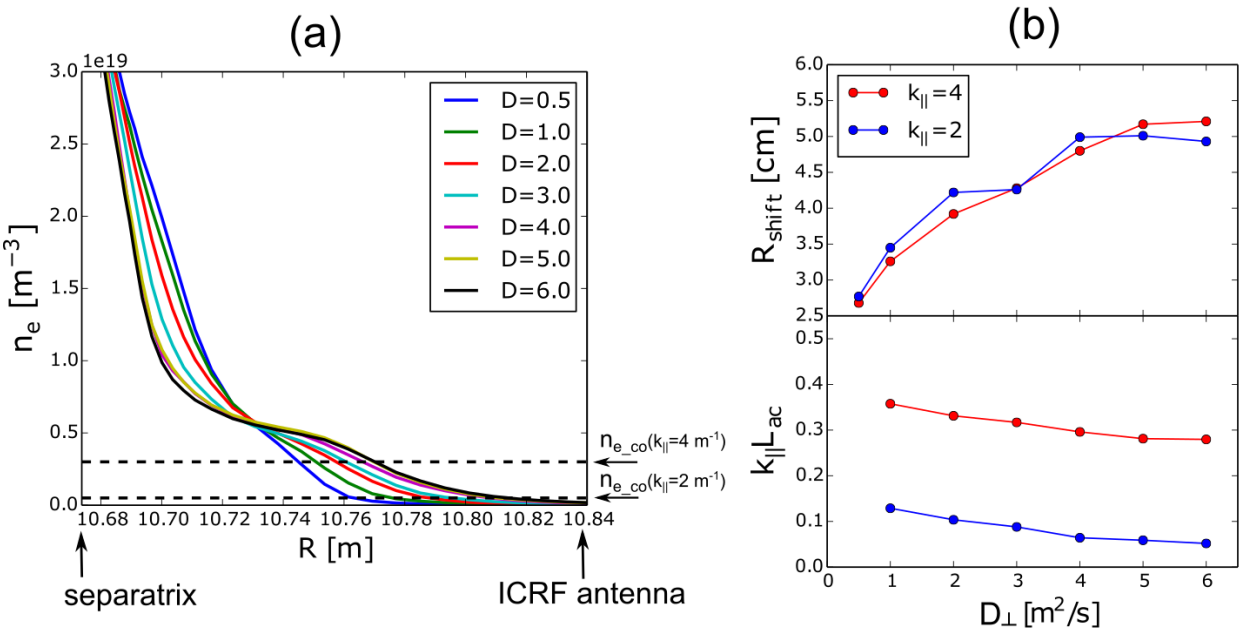

Figure 7. (a) A scan of $\mathrm{D}_\perp$ during antenna gas puffing. (b) The shift of the cut-off density position (R_{shift}) and $k_{||}L_{ac}$ as a function of particle transport coefficient $\mathrm{D}_\perp$.

3.5 Power flux to the main chamber wall

Local gas puffing influences the SOL density and temperature locally in locations close to the gas valve. As a result, the local particle and power fluxes to the main chamber wall are changed. To understand this, plasma density and temperature close to the top of vessel during divertor gas puffing and antenna gas puffing are compared, as shown in figure 8. It is can be seen that antenna gas puffing increases the local SOL density and decreases the local SOL temperature near the top of the vessel more than divertor gas puffing. The local SOL temperature decreases due to local ionization and pressure conservation. Gas puffing provides a local particle source. In a steady state, the ionized particles (ions and electrons) leave this ionization zone mainly via convection along the field lines. The associated convective energy flux and the power losses into the ionization processes provide an energy sink to the background plasma and thereby lower the plasma temperatures in the ionization region due to the finite classical heat conductivity, resulting in a local density rise as a consequence of the parallel pressure conservation [31].

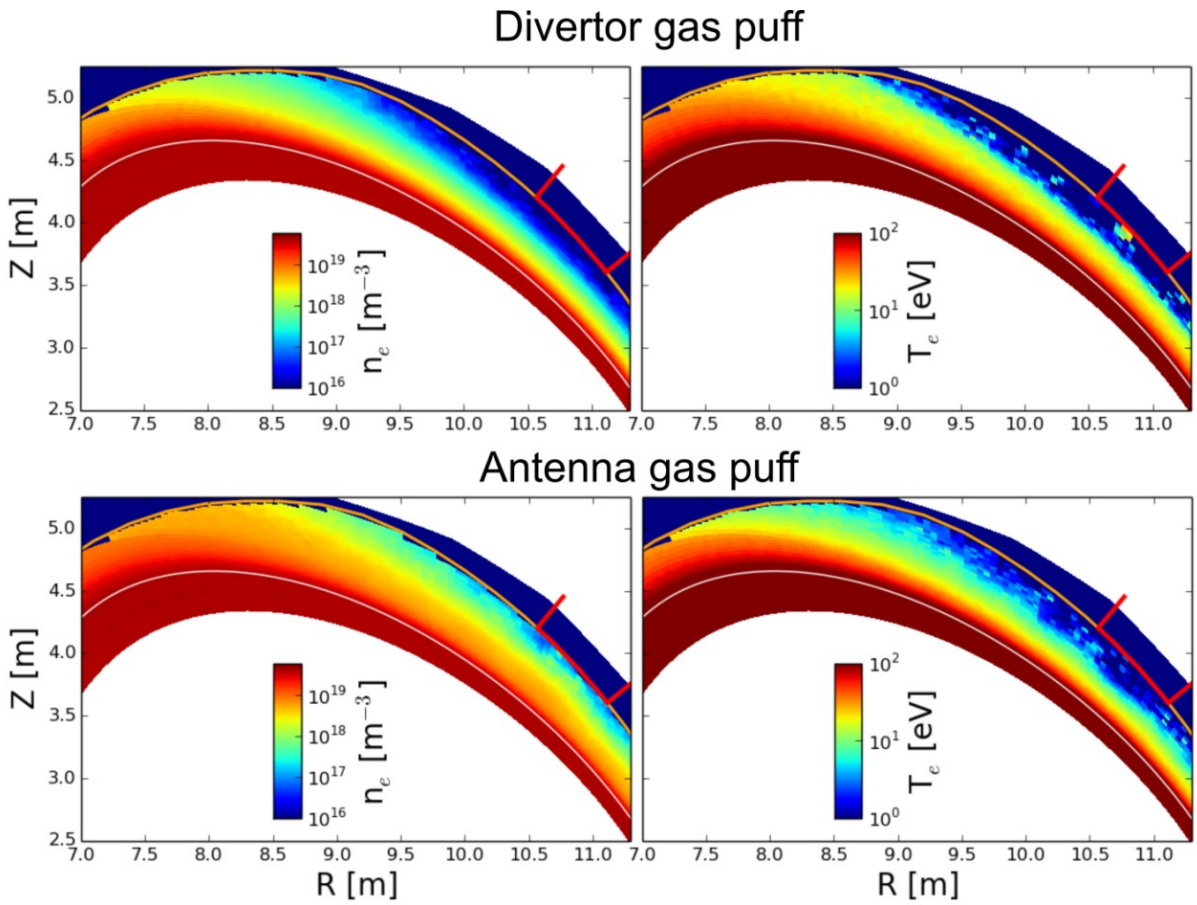

Figure 8. Plasma density and temperature near the top of main chamber wall during divertor gas puffing and antenna gas puffing, respectively.

The particle and power fluxes to the wall depend on the local density and temperature. The particle flux (i.e. the ion saturation current) is equal to $j = n_e v$, in which the electron velocity is proportional to the square root of temperature, $v \sim T_e^{1/2}$. This means that the particle flux has a stronger dependence on density than temperature. The power flux (i.e. the heat load on the wall) is proportional to the product of ion saturation current and temperature, i.e. $P = \gamma j k_B T_e$. Here γ is the sheath heat transmission coefficient. Subsequently one gets $P \sim n_e T_e^{3/2}$. This indicates that the power flux has a stronger dependence on temperature than density.

The top of the main chamber wall is relatively close to the plasma for the equilibrium used and receives a large power fluxes at the level of 10kW/m^2. Though this value is significantly smaller than the heat load on the divertor targets (in the level of 10MW/m^2), it is a contribution of about 10% to the main chamber wall assuming a limit of 1 MW/m^{-2}. The power flux to the upper part of the main chamber during divertor, top and antenna gas puffing is shown in figure 9. Compared to divertor gas puffing, antenna gas puffing decreases the peak heat load by ~33% and top gas puffing decreases this value by ~50%. This local heat load decrease is mainly due to a local decrease of the plasma temperature.

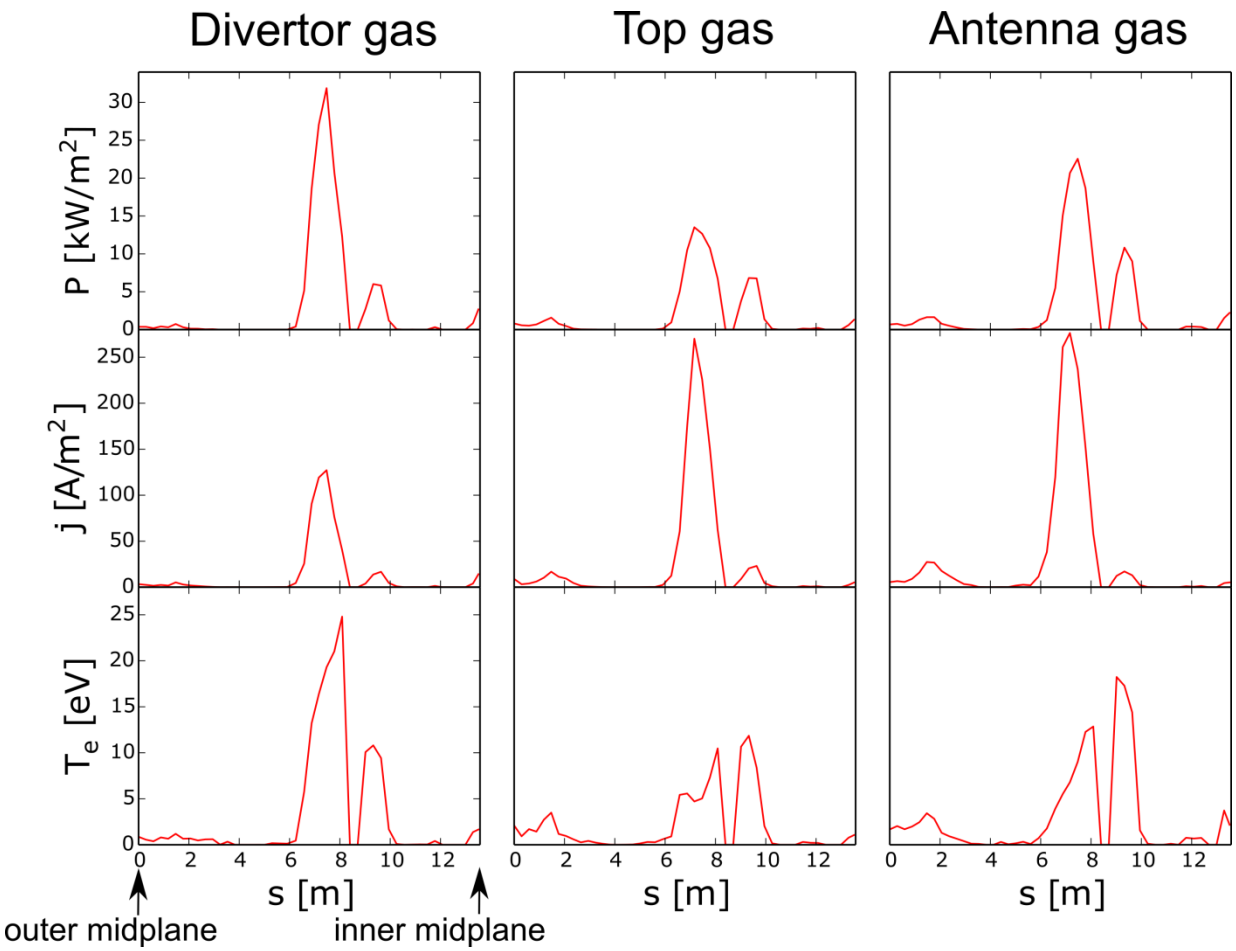

Figure 9. Power fluxes, particle fluxes and electron temperature on the upper part of the first wall during divertor gas puffing, top gas puffing and antenna gas puffing, respectively. The x-axis represents the distance from the outer midplane to the inner midplane in the counter-clockwise direction along the first wall.

4. Conclusion and Outlook

This paper presents the first EMC3-EIRENE simulation results of DEMO. It is shown that antenna gas puffing is a very powerful method to increase the antenna density and improve the ICRF coupling in DEMO. For the simulations, only one tokamak segment has to be simulated because the distributed traveling wave antenna and the toroidal distributed local gas valves are toroidally 18-fold symmetric. Effects of the divertor, top, midplane and antenna gas puffs on the SOL density and ICRF coupling have been studied. The results indicate that toroidally equally distributed and poloidally localized antenna gas puffing increases the SOL density in front of the antenna most significantly. Top or midplane gas puffing increases the SOL density but only to a moderate level. The spreading of neutral gas inside the main chamber wall plays a dominant role in increasing the local SOL density.

The increase of antenna density leads to the shift of the cut-off density position to the antenna. For antenna gas puffing, this shift depends almost linearly on the gas puff rate. The gas puff rate required for significant antenna density increase is in the level of $1 \times 10^{23} el/s$. With a total gas puff rate of $4 \times 10^{23} el/s$ (~4.4% of the total recycling flux), the shift of fast wave ($k_{||}$ = 2 m^{-1}) cut-off density position to the antenna is ~8 cm and the evanescent layer almost vanishes. This suggests that the ICRF coupling issue at the plasma edge can be very well solved with a proper gas puff rate. Antenna gas puffing is demonstrated to be a very efficient way to improve ICRF coupling in DEMO.

Moreover, influences of particle transport coefficient ($D_{\perp}$) on the SOL density in front of the antenna have been investigated with parameter scans. It is suggested that $D_{\perp}$ in the far SOL only has an influence on the SOL density profiles when it is lower than $4\ m^2/s$. Particle and power fluxes to the upper vessel are compared for different gas puffing cases. It is shown that antenna gas puffing decreases the power load on the main chamber wall locally due to a local reduction of plasma temperature near the gas valve.

In the paper, eighteen toroidally distributed gas valves near the antenna are considered for the traveling wave antenna. Future studies will investigate whether a reduction of the number of gas valves appears feasible. Since the density is most significantly increased in toroidal positions close to the gas valves, reducing the number of gas valves will lead to density inhomogeneities. Antenna locations toroidally far away from valves may be prone to insufficient ICRF coupling.

This paper clearly demonstrates the merits of local gas puffing in terms of improving ICRF coupling in DEMO. In the near future, we plan to calculate the antenna coupling resistances with the TOPICA or ANTITER code when the DEMO antenna design is accomplished. For this, the antenna density profiles calculated by EMC3-EIRENE as presented will be used as input parameters. Previously some exercises were done to calculate the radiation resistances for the DEMO antenna but with the ITER density profiles [12]. Our future work is expected to give more quantitative predictions of ICRF coupling increase with local gas puffing.

Acknowledgments: This work has been carried out within the framework of the EUROfusion Consortium and has received funding from the Euroatom research and training programme 2014-2018 under grant agreement No 633053. The views and opinions expressed herein do not necessarily reflect those of the European Commission.

References

[1] Bachmann C. *et al* 2015 *Fusion Engineering and Design* **98-99** 1423-6
[2] Tran M. Q. *et al* "EU DEMO Heating and Current Drive: Physics and Technology" *26th IAEA Fusion Energy Conference (Kyoto, Japan 2016)*
[3] Mikkelsen D. R. *et al* 2018 *Nuclear Fusion* **58** 036014
[4] Becoulet A. 1996 *Plasma Physics and Controlled Fusion* **38** A1-A11
[5] Jacquinot J. *et al* 1999 *Nuclear Fusion* **39** 2495-539
[6] Kazakov Y. O. *et al* 2015 *Plasma Physics and Controlled Fusion* **57** 025014
[7] Wauters T. *et al* 2015 *Journal of Nuclear Materials* **463** 1104-8
[8] Lerche E. *et al* 2016 *Nuclear Fusion* **56** 036022
[9] Bhatnagar V. P. *et al* 1994 *Nuclear Fusion* **34** 1579-603
[10] Eriksson L. G. *et al* 2004 *Physical Review Letters* **92** 235004
[11] Ragona R. *et al* 2016 *Nuclear Fusion* **56** 076009
[12] Messiaen A. *et al* 2016 *EPS conference Leuven* P2.066
[13] Ragona R. *et al* 2017 *EPJ Web of Conferences* **157** 03044
[14] Bader A. *et al* 2017 *Fusion Engineering and Design* **123** 431-4
[15] Garcia A. *et al* 2015 *Radiofrequency Power in Plasmas* **1689** 070002
[16] Bobkov V. *et al* 2014 *AIP Conference Proceedings* **1580** 271
[17] Zhang W. *et al* 2016 *Nuclear Fusion* **56** 036007
[18] Zhang W. *et al* 2017 *Nuclear Fusion* **57** 056042
[19] Jacquet P. *et al* 2016 *Nuclear Fusion* **56** 046001
[20] Zhang W. *et al* 2017 *Plasma Phys. Control. Fusion* **59** 075004
[21] Zhang W. "Scrape-off layer density tailoring with local gas puffing to maximize ICRF power coupling in ITER" *International Conference on Plasma Surface Interactions in Controlled Fusion Devices (Princeton, USA 2018)*
[22] Colas L. *et al* 2007 *Plasma Physics and Controlled Fusion* **49** B35-B45
[23] Zhang W. *et al* 2016 *Plasma Phys. Control. Fusion* **58** 095005
[24] Van Eester D. *et al* 2013 *Plasma Physics and Controlled Fusion* **55** 025002
[25] Tripský M. *et al* Monte Carlo simulation of ICRF discharge initiation at $\omega_{LHR} < \omega$ *41st EPS Conference on Plasma Physics (Berlin, Germany 2014)* P1.133
[26] Feng Y. *et al* 2004 *Contributions to Plasma Physics* **44** 57-69
[27] Reiter D. *et al* 2005 *Fusion Science and Technology* **47** 172-86
[28] Feng Y. *et al* 2014 *Contributions to Plasma Physics* **54** 426-31
[29] Ploeckl B. *et al* 2017 *Fusion Engineering and Design* **123** 186-91
[30] Stix T. H. 1992 *Waves in Plasmas* American Inst. of Physics
[31] Zhang W. *et al* 2017 *EPJ Web of Conferences* **157** 03066